

Quantum order by disorder in frustrated diamond lattice antiferromagnets

Jean-Sébastien Bernier,¹ Michael J. Lawler,¹ and Yong Baek Kim¹

¹*Department of Physics, University of Toronto, Toronto, Ontario M5S 1A7, Canada*

(Dated: March 25, 2019)

We present a quantum theory of frustrated diamond lattice antiferromagnets. Considering quantum fluctuations as the predominant mechanism relieving spin frustration, we find a rich phase diagram comprising of six phases with coplanar spiral ordering in addition to the Néel phase. By computing the specific heat of these ordered phases, we obtain a remarkable agreement between $(k, k, 0)$ -spiral ordering and the experimental specific heat data for the diamond lattice spinel compounds MnSc_2S_4 , Co_3O_4 and CoRh_2O_4 , *i.e.* *specific heat data* is a strong evidence for $(k, k, 0)$ -spiral ordering in all of these materials. This prediction can be tested in future neutron scattering experiments on Co_3O_4 and CoRh_2O_4 , and may also be consistent with the existing neutron scattering data on MnSc_2S_4 . Furthermore, based on this agreement we infer a monotonically increasing relationship between frustration and the strength of quantum fluctuations.

Introduction. In insulating magnetic materials, new phases of matter may be found by letting local exchange interactions compete. In such situations, the spins are said to be frustrated and intriguing new phases such as ordered phases with coplanar or spiral ordering or “spin liquid” paramagnets can arise.[1] In any given frustrated material, the ground state may be determined by identifying the primary mechanism relieving the frustration. While extrinsic mechanisms, such as small dipole interactions[2], disorder or lattice distortions[3], may be important, perhaps the most interesting possibility is when temperature or quantum fluctuations alone relieve the frustration, a process termed “order by disorder”.[4]

In this light, recent experiments which unveil strong frustration in spinel compounds AB_2X_4 , with magnetic ions occupying the A-sites, are particularly interesting. Here the A-sites form a diamond lattice of spin $S = \frac{3}{2}, 2, \frac{5}{2}$ local moments. Important examples include seven diamond spinels[5], four that order: MnSc_2S_4 ; MnAl_2O_4 ; Co_3O_4 ; CoRh_2O_4 and three that do not down to the lowest temperatures studied: CoAl_2O_4 ; FeAl_2O_4 ; FeSc_2S_4 . When the moments order, the ordering temperature, T_c , is low compared to the Curie-Weiss temperature, Θ_{CW} , with frustration parameters[6], $f = \frac{|\Theta_{\text{CW}}|}{T_c}$, varying from 1.2 to 10. The magnetic ordering in one of the ordered materials, MnSc_2S_4 , has been identified as an exotic $(k, k, 0)$ coplanar spiral via extensive neutron scattering experiments[5] while the magnetic ordering patterns of other ordered diamond spinels are not determined yet. Given that a diamond lattice is bipartite, this ubiquitous evidence for frustration is highly unexpected.

In combination with their frustrated magnetic properties, diamond spinels also have unusual temperature dependence of specific heat. Remarkably, among the four materials that order, their specific heat data share the same unusual behavior below T_c (see Ref.[5]). Instead of a pure T^3 power-law expected for incommensurate magnetic ordering in three dimensions, two inflection points are observed. The three that do not order also share the same characteristic specific heat, but is quite different from those that order. These materials display a $T^{2.5}$ power-law over a decade in temperature.[5]

Following these experimental discoveries, the classical Heisenberg model on the diamond lattice with the nearest

and next-nearest neighbor exchange interactions has been studied[7]. It was demonstrated that the frustration arises from the next-nearest neighbor interactions that couple spins within each of the two face-centered cubic (FCC) sublattices of the diamond lattice structure[7]. This coupling creates a highly degenerate set of classical coplanar spirals whose propagation vectors form a continuous surface in momentum space. Relieving this classical ground state degeneracy by thermal fluctuations was then found to produce a rich phase diagram at the classical level[7], including the $(k, k, 0)$ spiral phase discovered in the neutron scattering experiments on MnSc_2S_4 . This put diamond spinels in a promising class of materials in which (thermal) “order by disorder” may be experimentally observed. However, this classical picture may not be sufficient to describe possible effect of quantum fluctuations in these materials with relatively small spin $S = \frac{3}{2}, 2, \frac{5}{2}$ and the specific heat data below T_c .

In this letter, we present a quantum theory of frustrated diamond lattice antiferromagnets. We find that quantum fluctuations act as an order by disorder mechanism to produce a similar but richer phase diagram compared with that obtained exclusively from thermal fluctuations. In particular, focusing on the ordered states, we demonstrate that the characteristic signatures in the specific heat data of three of the ordered materials (MnSc_2S_4 , Co_3O_4 and CoRh_2O_4) can be explained if the magnetic ordering pattern in these materials is $(k, k, 0)$ -spiral selected by strong quantum fluctuations. Thus, we argue that specific heat data is a convincing evidence for $(k, k, 0)$ -spiral ordering in all these materials. Based on this comparison, we show how frustration and quantum fluctuations are strongly intertwined in these systems. Finally, we discuss the implications of our results on future neutron scattering experiments on these materials.

Keeping in mind that frustration arises from the next-nearest neighbor exchange interactions[7], we begin with the following quantum Heisenberg model:

$$H = J_1 \sum_{\langle ij \rangle} \mathbf{S}_i \cdot \mathbf{S}_j + J_2 \sum_{\langle\langle ij \rangle\rangle} \mathbf{S}_i \cdot \mathbf{S}_j, \quad (1)$$

where \mathbf{S}_i are spin- S operators at site i , $J_1 > 0$ is the exchange coupling on the nearest-neighbor links (between sites on dif-

ferent FCC sublattices) and $J_2 > 0$ is the exchange coupling on the next-nearest-neighbor links (between sites on the same FCC sublattice). By studying the large- N limit of the $\text{Sp}(N)$ generalization of this model[8], we study the role of quantum fluctuations as a controlled expansion in $\frac{1}{N}$. The advantage of this method is that, unlike the large- S expansion[9], the results are non-perturbative in the spin magnitude S (strength of quantum fluctuations) and the coupling constants (J_1 and J_2). The resulting phase diagram, which indeed exhibits order by disorder, is presented in Fig.1. For $\frac{J_2}{J_1} > 1/8$, the energy of the degenerate set of classical states is given by the grey-to-black pixellated surface on the right hand side of the figure. Zero point energy corrections due to quantum fluctuations lift this degeneracy (grey-to-black pixels represent higher-to-lower energy spin configurations) and only the black pixels with the smallest energy remain degenerate. The phase diagram was obtained based on the resulting magnetic order of the selected ground state.

Fig.1 also shows clearly that quantum and thermal fluctuations lift the classical ground state degeneracy differently. Comparing our results with a study where only entropic effects were considered[7], we notice that both kinds of fluctuations select states along similar high symmetry directions such as (k, k, k) , $(k, k, 0)$ and $(k, 0, 0)$. However, similar states are not always present in the same range of $\frac{J_2}{J_1}$ ratios. In addition, we find within numerical accuracy that quantum fluctuations do not always lift the degeneracy, or lift it only partly as in the “degenerate”, “circle” and “cross” phases. This is in contrast to thermal fluctuations, where points of lowest energy are always selected when entropic effects are considered.

Focusing on the diamond spinels that magnetically order at low temperatures, we find remarkable agreement between the measured heat capacity and our large- N theory in a phase with $(k, k, 0)$ ordering. As shown in Fig.2, $\frac{C}{T}$ for CoRh_2O_4 , Co_3O_4 and MnSc_2S_4 , have two characteristic inflection points before reaching T_c , a feature that is best reproduced by the $(k, k, 0)$ spiral ordering in the large- N limit. Consequently, we propose that all of these spinels most likely have $(k, k, 0)$ spiral ordering. This result is in agreement with neutron scattering experiments on MnSc_2S_4 . [5] Future neutron scattering experiments on CoRh_2O_4 and Co_3O_4 could verify this prediction.

Through the remarkable fitting of the large- N theory to the heat capacity data, we also find a simple relationship between the empirical frustration parameter, f , and the strength of quantum fluctuations given by the large- N effective spin length parameter $\kappa = \frac{2S_{\text{eff}}}{N}$ (here κ is held fixed in the $N \rightarrow \infty$ limit). To describe adequately the experimental specific heat data of the more frustrated (larger f) compounds, we need to include stronger quantum fluctuations than required to describe the moderately frustrated ones. As shown in Fig.2, the spin $\frac{5}{2}$ system MnSc_2S_4 with frustration parameter $f = 10$ is best fitted using $\kappa = 1.7$ while the spin $\frac{3}{2}$ system CoRh_2O_4 with $f = 1.2$ is best fitted with $\kappa = 2.5$. Thus for the diamond spinels that order at low temperatures, quantum fluctuations correlate with frustration much more than with the physical spin representation.

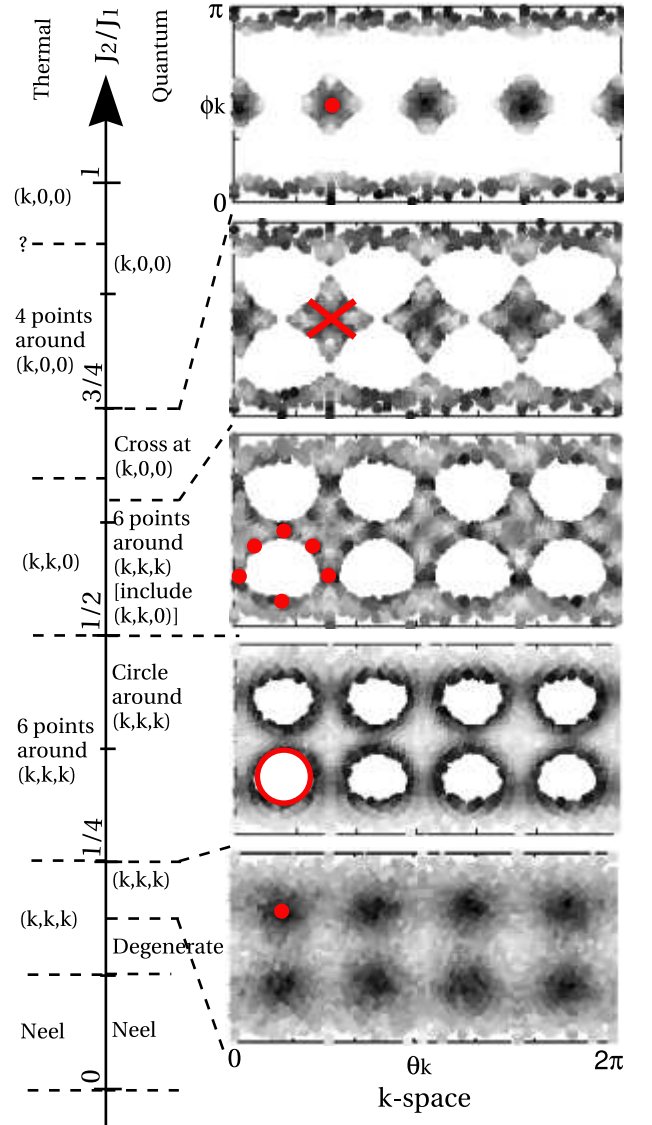


FIG. 1: Structure of the ground states as a function of $\frac{J_2}{J_1}$ after the inclusion of quantum fluctuations. The ϕ_k versus θ_k plots on the right are planar views of the somewhat distorted and/or punctured sphere forming the set of degenerate classical ground states. Darker points represent lower energy. On each plot, red dots or lines give examples of states selected by quantum fluctuations. To contrast the effects of quantum and thermal fluctuations, states selected by entropic effects are summarized on the left.[7]

In the sections to follow, we present in detail how the results stated above were obtained.

General $\text{Sp}(N)$ mean-field free energy. The Hamiltonian describing the interactions between spins on the diamond lattice is given by Eq.1. The $\text{SU}(2)$ spin symmetry of the Hamiltonian is generalized to $\text{Sp}(N)$ by first recasting the spins using the bosonic representation $\vec{S}_i = \frac{1}{2}b_{i\alpha}^\dagger \vec{\sigma}_{\alpha\beta} b_{i\beta}$ where $\alpha, \beta = \{\uparrow, \downarrow\}$ labels two possible spin states of each boson and then by introducing N flavors of such bosons on each site. In order to keep the physical Hilbert space of spins, a constraint on the number of bosons given by $n_b = b_{i\alpha}^\dagger b_{i\alpha}^m =$

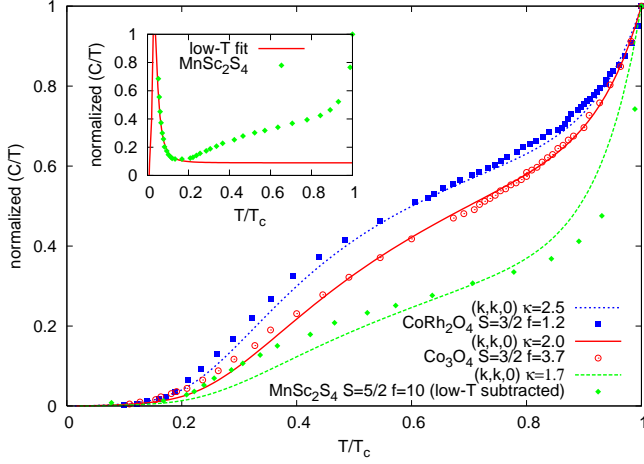


FIG. 2: Comparison of specific heat data of CoRh_2O_4 , Co_3O_4 , MnSc_2S_4 and the theoretical large- N specific heat of the $(k, k, 0)$ spiral ordering with $J_2/J_1 = 0.6$. Here $1/\kappa = N/2S_{\text{eff}}$, held fixed in the large- N limit, gives the strength of quantum fluctuations and increases monotonically with the frustration parameter $f = |\Theta_{\text{CW}}|/T_c$. The inset shows the subtraction of the nuclear contribution with a constant “background” from the specific heat of MnSc_2S_4 using $C_I/T = \Delta^2/T^3(e^{\Delta/T})/(1 + e^{\Delta/T})^2 + C_0$.

$2S_{\text{eff}} = \kappa N$ where $m = 1, \dots, N$ must be imposed at each site. Note that $N = 1$ corresponds to the physical limit $\text{Sp}(1) \equiv \text{SU}(2)$. The action of the corresponding $\text{Sp}(N)$ generalized model is then given by

$$\mathcal{S} = \int_0^\beta d\tau \{ \bar{b}_{i\alpha}^m \partial_\tau b_{i\alpha}^m - \frac{J_{ij}}{2N} \bar{A}_{ij} A_{ij} + \lambda_i (\bar{b}_{i\alpha}^m b_{i\alpha}^m - n_b) \} \quad (2)$$

where $A_{ij} = \epsilon_{\alpha\beta} \delta_{mm'} b_{i\alpha}^m b_{j\beta}^{m'}$ ($\epsilon_{\alpha\beta} \delta_{mm'}$ is the $\text{Sp}(N)$ generalized antisymmetric tensor of $\text{SU}(2)$) and the chemical potential λ_i keeps the average number of bosons fixed to $n_b = \kappa N$ at every site. The mean-field action is then obtained by decoupling the quartic boson interaction in \mathcal{S} using the Hubbard-Stratonovich fields $Q_{ij} = -Q_{ji}$ directed along the lattice links so that one obtains $Q_{ij} = \langle A_{ij} \rangle / N$ at the saddle point. The mean field solution becomes exact in the large- N limit where $N \rightarrow \infty$ is taken while $\kappa = n_b/N$ is fixed. We also introduce the parameterization $b_{i\alpha}^m = (\sqrt{N} x_{i\alpha} b_{i\alpha}^{\tilde{m}})^T$ where $\tilde{m} = 2, \dots, N$ to allow for the possibility of long-range order that occurs when $x_{i\alpha} \neq 0$. Consequently, after integrating over the bosons, and rescaling Q_{ij} and λ by κ , $x_{i\alpha}$ by $\sqrt{\kappa}$ and the temperature by κ^2 , we obtain the mean-field free energy

$$\begin{aligned} \frac{F}{N\kappa^2} &= \sum_{i,j} \frac{J_{ij}}{2} (|Q_{ij}|^2 - Q_{ij}(\epsilon_{\alpha\beta} x_{i\alpha}^* x_{j\beta}^*) + c.c.) \\ &+ \lambda \sum_i (|x_{i\alpha}|^2 - (\frac{1}{\kappa} + 1)) + f_{\text{eff}} \end{aligned} \quad (3)$$

where $f_{\text{eff}} = \sum_\mu \frac{\omega_\mu(Q, \lambda)}{\kappa} + 2k_B T \ln(1 - e^{-\frac{\omega_\mu(Q, \lambda)}{\kappa k_B T}})$ where $\omega_\mu(Q, \lambda)$ are the eigenvalues of the mean-field Hamiltonian. Note that the chemical potential is now taken to be uniform

since each site has the same number of nearest neighbor and next nearest neighbor links. In general, magnetic ordering $x_{i\alpha} \neq 0$ occurs in the semiclassical limit at larger κ while quantum paramagnetic phases are obtained when κ is small.

Classical ground state. In the classical limit $\kappa \rightarrow \infty$ at $T \rightarrow 0$, one can show that $Q_{ij}^c = \epsilon_{\alpha\beta} x_{i\alpha}^c x_{j\beta}^c$, so that the classical energy is given by

$$\frac{E^c}{N\kappa^2} = - \sum_{i,j} \frac{J_{ij}}{2} |\epsilon_{\alpha\beta} x_{i\alpha}^c x_{j\beta}^c|^2 + \lambda^c \sum_i (|x_{i\alpha}^c|^2 - 1). \quad (4)$$

Minimizing this expression with respect to $x_{i\alpha}^c$ and λ^c is equivalent to determining the classical ground states of Eq.1 provided the solution has $|x_{i\alpha}^c|^2 = 1$. Rewriting E^c in terms of a quadratic form in the classical unit spin vectors $\vec{S}_i^c = x_{i\alpha}^c \vec{\sigma}_{\alpha\beta} x_{i\beta}^c$ and transforming to momentum space unveils two bands with energy

$$\epsilon_\pm(\mathbf{k}) = J_2(\Lambda^2(\mathbf{k}) - 1) \pm \frac{1}{2} J_1 \Lambda(\mathbf{k}) \quad (5)$$

where $\Lambda^2(\mathbf{k}) = 4\{\prod_{u=x,y,z} \cos^2 \frac{k_u}{4} + \prod_{u=x,y,z} \sin^2 \frac{k_u}{4}\}$. The minimum eigenvalue is obtained in the lower band ϵ_- and is unique at $\mathbf{k} = 0$ for $J_2/J_1 < 1/8$ but highly degenerate, corresponding to a surface in momentum space, for $J_2/J_1 \geq 1/8$. For $1/8 \leq J_2/J_1 \leq 1/4$, the space of ground states resembles the surface of a slightly deformed sphere. For larger J_2/J_1 , the size of the “sphere” increases and eight holes centered around the (k, k, k) directions begin to puncture its surface (see also Ref.[7]). The solution of the classical limit is then completed by finding for each degenerate eigenstate, labeled by its \mathbf{k} value, its corresponding real space spin configuration and chemical potential. In terms of our spinor representation, we obtain $x_{i\uparrow/\downarrow}^{c,A} = \pm \frac{1}{\sqrt{2}} e^{\mp \frac{i}{2}(\mathbf{k} \cdot \mathbf{r}_i - \frac{1}{2}\theta(\mathbf{k}))}$ and $x_{i\uparrow/\downarrow}^{c,B} = \frac{1}{\sqrt{2}} e^{\mp \frac{i}{2}(\mathbf{k} \cdot \mathbf{r}_i + \frac{1}{2}\theta(\mathbf{k}))}$ where A and B label the two interpenetrating FCC sublattices and $\theta(\mathbf{k}) = \arctan(\tan \frac{k_x}{4} \tan \frac{k_y}{4} \tan \frac{k_z}{4})$. Varying E^c with respect to λ^c then gives the corresponding chemical potential $\lambda_i^c = \frac{1}{x_{i\uparrow}^{c*}} \sum_j \frac{J_{ij}}{2} Q_{ij}^{c*} x_{j\downarrow}^c$ and is the same on all lattice sites.

Effect of quantum fluctuations. Given the above solution to the classical ground states, consider expanding the ground state energy E in powers of $1/\kappa$ so that $E = E^c + \frac{1}{\kappa} E^1 + \dots$. This leads to the quantum correction

$$\frac{E^1}{N\kappa^2} = \sum_\mu \omega_\mu(Q^c, \lambda^c) - \lambda^c N_S \quad (6)$$

where N_S is the number of lattice sites and Q^c , the classical values for the link variables, are given by $Q_{ij}^{c,AA/BB} = \mp i \sin(\frac{\mathbf{k} \cdot (\mathbf{r}_j - \mathbf{r}_i)}{2})$ and $Q_{ij}^{c,AB/BA} = \pm \cos(\frac{\mathbf{k} \cdot (\mathbf{r}_j - \mathbf{r}_i) \pm \theta(\mathbf{k})}{2})$. Since Q_{ij}^c is only dependent on the difference between two sites, we can Fourier transform back to momentum space and solve for E^1 analytically as a sum over wave-vectors. In practice, this energy correction is computed using an adaptive Monte Carlo integration method and the new ground state is found by sampling the surface of equal energy. The first order quantum corrections dramatically alter the topology of the

degenerate ground state manifold reducing the k -space surface of lowest energy to only points or lines of lowest energy represented by the black pixels in Fig.1.

The effect of quantum fluctuations, depicted in Fig.1, can be summarized as follows: for $0.125 < \frac{J_2}{J_1} < 0.18$, the “sphere” of equal energy remains surprisingly degenerate; for $0.18 < \frac{J_2}{J_1} < 0.25$, the eight (k, k, k) directions are selected; for $0.25 < \frac{J_2}{J_1} < 0.5$, states labeled by k points forming eight circles around the (k, k, k) directions are chosen; for $0.5 < \frac{J_2}{J_1} < 0.65$, each circle gives way to six points around each (k, k, k) direction (among which three points are $(k, k, 0)$ directions); for $0.65 < \frac{J_2}{J_1} < 0.75$, the states labeled by k points form a degenerate cross centered around each $(k, 0, 0)$ direction and finally for $\frac{J_2}{J_1} > 0.75$ states labeled by points along the six $(k, 0, 0)$ directions become the states of lowest energy.

Specific heat and comparison to experiments. To compare the above order by disorder predictions with current experiments, we compute the specific heat. Extending the formalism to finite temperatures, we assume that the phase and amplitude of both bond variables and condensates can vary but that these changes are spatially uniform. We write Q_{ij} and $x_{i\alpha}$ as

$$Q_{ij} = R(T) e^{i\xi} Q_{ij}^c, \quad x_{i\alpha} = \sqrt{r(T)} e^{i\zeta} x_{i\alpha}^c, \quad (7)$$

where Q_{ij}^c and $x_{i\alpha}^c$ are bond and condensate values in one of the $T = 0$ spin configurations chosen by quantum fluctuations. For a given temperature, T , and effective spin length parameter, κ , $R(Q, \lambda, T)$, $r(Q, \lambda, T)$, ξ and ζ are obtained from self-consistent saddle point equations. In the cases of spiral configurations (k, k, k) , $(k, k, 0)$ and $(k, 0, 0)$, the ground state is magnetically ordered at $T = 0$ if $\kappa > \kappa_c$ where, for example, $\kappa_c = 0.17, 0.094, 0.087$ for $\frac{J_2}{J_1} = 0.2, 0.6, 0.85$.

We use Eq.7 in the general free energy expression (Eq.3), and obtain the specific heat $C = -T \frac{\partial^2 F}{\partial T^2}$. In the limit of very low temperatures, $R(T)$ and $r(T)$ are approximately independent of temperature and $C \sim T^3$ as expected for three-dimensional antiferromagnets. However, as temperature is increased, the temperature dependence of R and r becomes important and the specific heat departs from its T^3 behavior. As shown in Fig.2, the specific heat obtained from the $(k, k, 0)$ spiral ordering with $\frac{J_2}{J_1} = 0.6$ agrees well with the experimental specific heat data of CoRh_2O_4 and Co_3O_4 and the fit looks reasonable for MnSc_2S_4 . For these three materials, $\frac{C}{T}$ presents two inflection points before T_c , a feature that is best reproduced by $(k, k, 0)$ ordering and is robust for a finite range of $\frac{J_2}{J_1}$ as long as the magnetic ordering remains the same. We find that other ordering wavevectors do not reproduce as nicely the characteristic temperature dependence of the specific heat data. Regarding MnSc_2S_4 , the low temperature part of the experimental specific heat has substan-

tial nuclear spin contributions that we subtract using a simple two-level system formula as described in the figure caption of Fig.2. Also, Ref.[7] pointed out that the neutron scattering experiment on this material suggests $\frac{J_2}{J_1} = 0.85$ and implies that a third neighbor coupling J_3 is necessary to stabilize $(k, k, 0)$ order for this value of $\frac{J_2}{J_1}$. We expect that the latter and the error arising from the subtraction of the nuclear contribution are the reasons behind the less satisfactory fit for MnSc_2S_4 .

Conclusion. In this work, we presented a theory of frustrated diamond lattice quantum antiferromagnets. Considering quantum fluctuations as the predominant mechanism relieving spin frustration in this spin system we found a rich phase diagram consisting of six phases with coplanar spiral ordering in addition to the Néel phase. By comparing specific heat curves found in the large- N mean-field theory with data obtained from CoRh_2O_4 , Co_3O_4 and MnSc_2S_4 , we propose that they all share the same magnetic order in their ground state: a coplanar spiral with propagation vector $(k, k, 0)$. Note that the neutron scattering data is currently available only for MnSc_2S_4 . From the fit in Fig.2, we conclude that a remarkable correlation exists between the strength of quantum fluctuations, measured by the effective spin magnitude $\kappa = \frac{2S_{\text{eff}}}{N}$, and the empirical frustration parameter $f = \frac{|\Theta_{\text{CW}}|}{T_c}$ while κ and the physical spin magnitude $S = \frac{3}{2}, \frac{5}{2}$ of the magnetic ions appear only loosely related. We expect future neutron scattering experiments will verify our predictions.

We would like to thank J. Alicea, D. Bergman, L. Balents, S. Takei and S. Trebst for helpful discussions. This work was supported by NSERC, CRC, CIFAR, KRF-2005-070-C00044 (JSB, MJL, YBK), and FQRNT and OGS (JSB).

-
- [1] For a review, see R. Moessner, Can. J. Phys. **79**, 1283 (2001).
 - [2] S.E. Palmer and J.T. Chalker, Phys. Rev. B **62**, 488 (2000).
 - [3] Y. Yamashita and K. Ueda, Phys. Rev. Lett. **85**, 4960 (2000); O. Tchernyshyov, R. Moessner, and S.L. Sondhi, Phys. Rev. Lett. **88**, 067203 (2002).
 - [4] J. Villain, R. Bidaux, J.-P. Carton and R. Conte, J. Physique **41**, 1263 (1980); E.F. Shender, Sov. Phys. JETP **56**, 178 (1982).
 - [5] V. Fritsch et al., Phys. Rev. Lett. **92**, 116401 (2004); A. Krimmel et al., Phys. Rev. B **73**, 014413 (2006); A. Krimmel et al., Phys. Rev. Lett. **94**, 237402 (2005); N. Tristan et al., Phys. Rev. B **72**, 174404 (2005); T. Suzuki et al., J. Phys. Condens. Matter **19**, 145265 (2007).
 - [6] A.P. Ramirez, Ann. Rev. Mat. Sc. **24**, 453 (1994).
 - [7] D. Bergman, J. Alicea, E. Gull, S. Trebst and L. Balents, Nature Physics **3**, 487 (2007).
 - [8] S. Sachdev, Phys. Rev. B **45**, 12377 (1992); N. Read and S. Sachdev, Phys. Rev. Lett. **66**, 1773 (1991).
 - [9] C. Henley, Phys. Rev. Lett. **62**, 2056 (1989).